

Fig. 3.4. The sky distribution, in Galactic coordinates, of 2704 GRBs detected with BATSE over 9+ years. The typical location error of these GRBs is several degrees. The color of each GRB location is indicative of its intensity, as indicated by the color bar at the bottom of the figure. (Credit: NASA.)

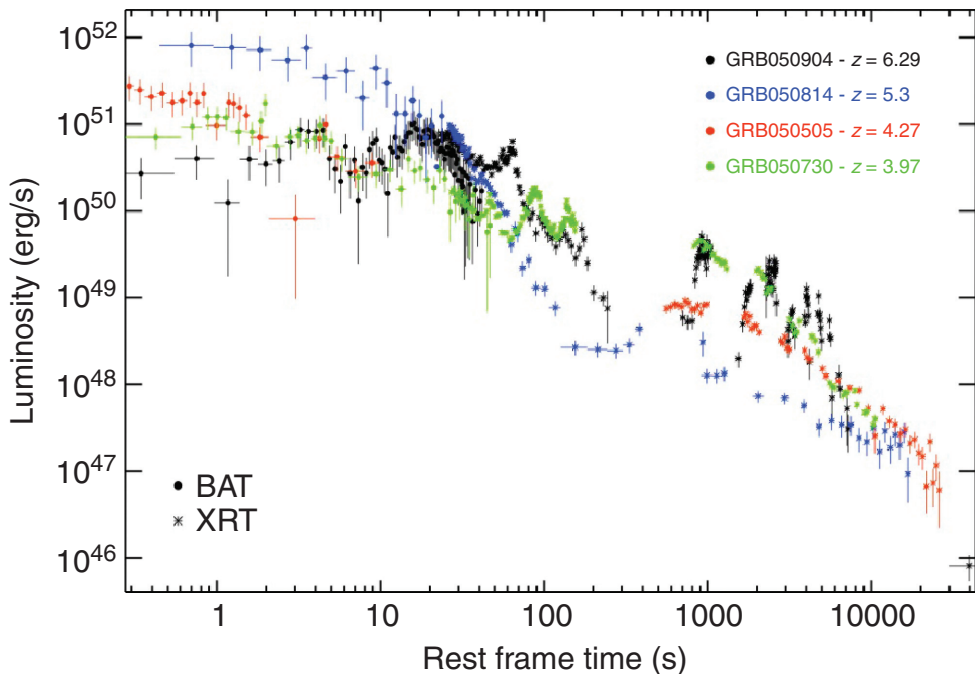


Fig. 5.11. Light curves (BAT–XRT) of four high- z *Swift* bursts (from Cusumano *et al.* (2007)). (Reproduced with permission © ESO.)

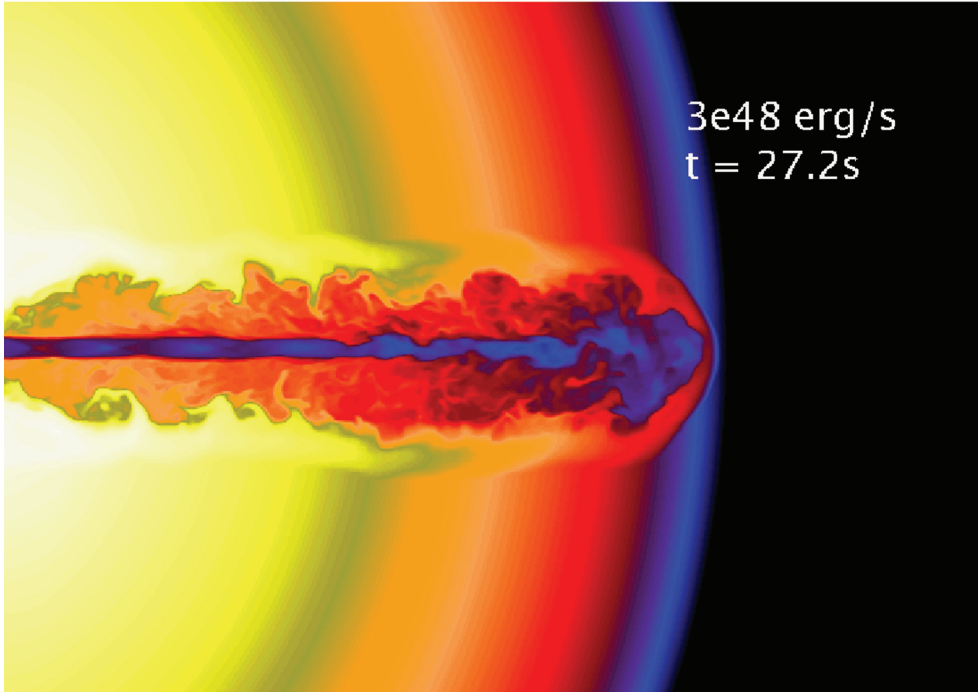


Fig. 10.1. Three-dimensional calculation by Weiqun Zhang of a relativistic jet of $3 \times 10^{48} \text{ erg s}^{-1}$ introduced at $1 \times 10^{10} \text{ cm}$ in a $15 M_{\odot}$ Wolf-Rayet pre-supernova star of radius $8 \times 10^{10} \text{ cm}$. Plotted is the logarithm of the density as the jet nears the surface. The jet took much longer to reach the surface than a similar jet with power $3 \times 10^{50} \text{ erg s}^{-1}$ studied by Zhang *et al.* (2004) and was less stable. After breakout, the jet eventually becomes more stable as an opening is cleared by the relativistic flow.

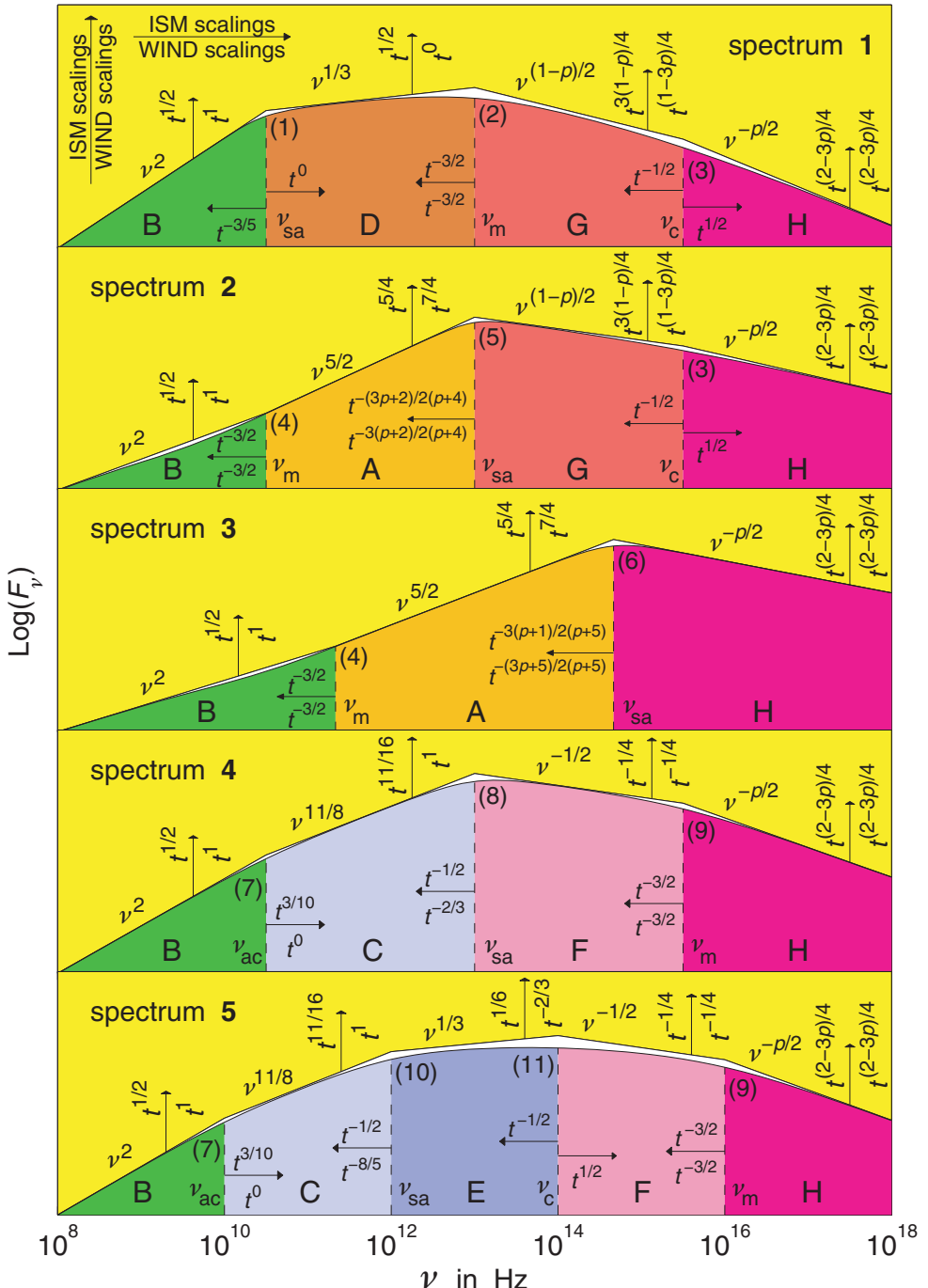


Fig. 11.3. The afterglow synchrotron spectrum, calculated for the Blandford and McKee (1976) spherical self-similar solution, under standard assumptions, using the accurate form of the synchrotron spectral emissivity and integration over the emission from the whole volume of shocked material behind the forward (afterglow) shock (for details see Granot & Sari 2002). The different panels show the five possible broadband spectra of the afterglow synchrotron emission, each corresponding to a different ordering of the spectral break frequencies. Each spectrum consists of several power-law segments (PLSs); each shown with a different color and labeled by a different letter A–H) that smoothly join at the break frequencies (numbered 1–11). The broken power-law spectrum, which consists of the asymptotic PLSs that abruptly join at the break frequencies (and is widely used in the literature), is shown for comparison. Most PLSs appear in more than one of the five different broadband spectra. Indicated next to the arrows are the temporal scaling of the break frequencies and the flux density at the different PLSs, for a uniform (ISM; $k = 0$) and stellar, wind (WIND; $k = 2$) external density profile. (Reproduced with permission from the AAS.)

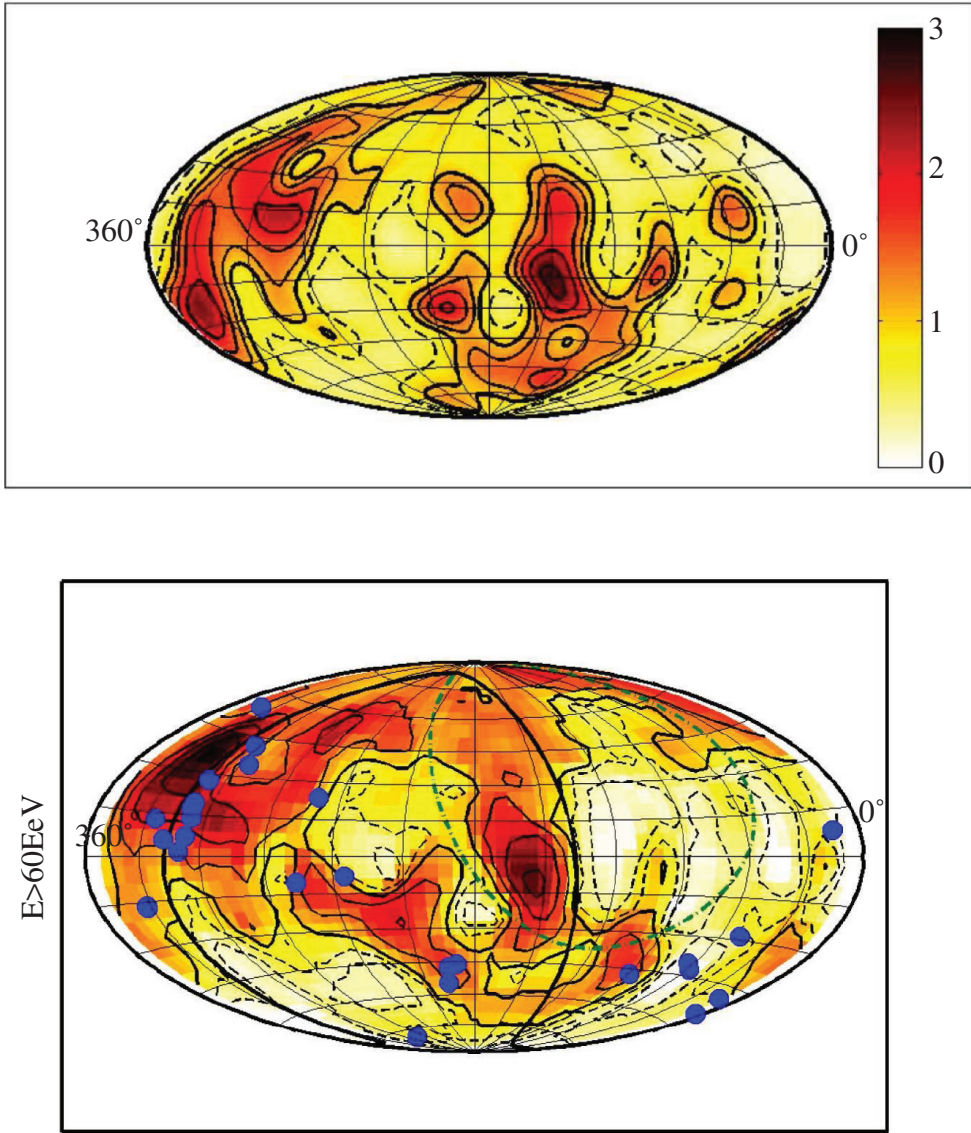


Fig. 12.4. *Top:* The integrated galaxy density out to a distance of 75 Mpc, normalized to the mean integrated density. The contours are logarithmic, ranging from 0.5 to 4 with three contours per density doubling. Dashed curves represent under-density. *Bottom:* The positions of the 27 Auger events with energy exceeding 5.7×10^{19} eV (Pierre Auger Collaboration, 2008), overlaid on the UHECR intensity map, $J(\hat{\Omega})$, predicted in a model in which the UHECR source distribution follows the galaxy density distribution (with a bias $b[\delta] = 1 + \delta$ for $\delta > 0$, $b = 0$ otherwise, where δ is the fractional galaxy over-density). The coordinates are Galactic and J is normalized to its all-sky average. The contours denote $J/\bar{J} = (0.7, 0.9, 1, 1.1, 1.3, 1.5)$, with dashed lines representing under-density. The solid green line denotes the super-Galactic plane. The dashed-dotted blue line marks the boundary of Auger's coverage (corresponding to a zenith angle of 60°). Adapted from Kashti & Waxman (2008).

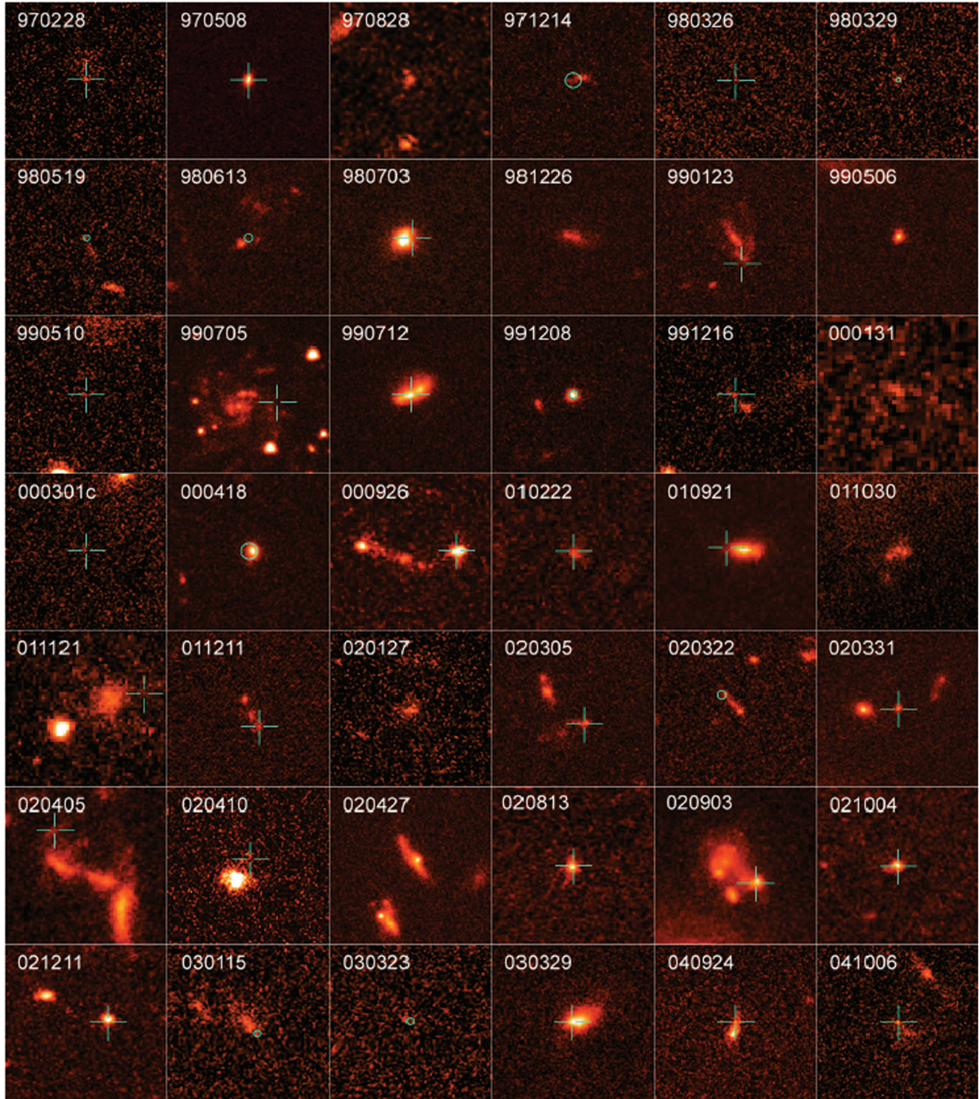


Fig. 13.4. A mosaic of GRB host galaxies imaged with *HST* (from Fruchter *et al.* 2006). Each individual image corresponds to a square region on the sky 3.75 arcsec on a side. These images were taken with the *HST*. In cases where the location of the GRB on the host is known to better than 0.15 arcsec, the position of the GRB on the host is shown by a green mark. If the positional error is smaller than the point spread function of the image (0.07 arcsec for STIS and ACS, 0.13 arcsec for WFPCC2) the position is marked by a cross-hair, otherwise the positional error is indicated by a circle. Due to the redshifts of the hosts, these images generally correspond to blue or ultraviolet images of the hosts in their rest frame, and thus detect light largely produced by the massive stars in the hosts.

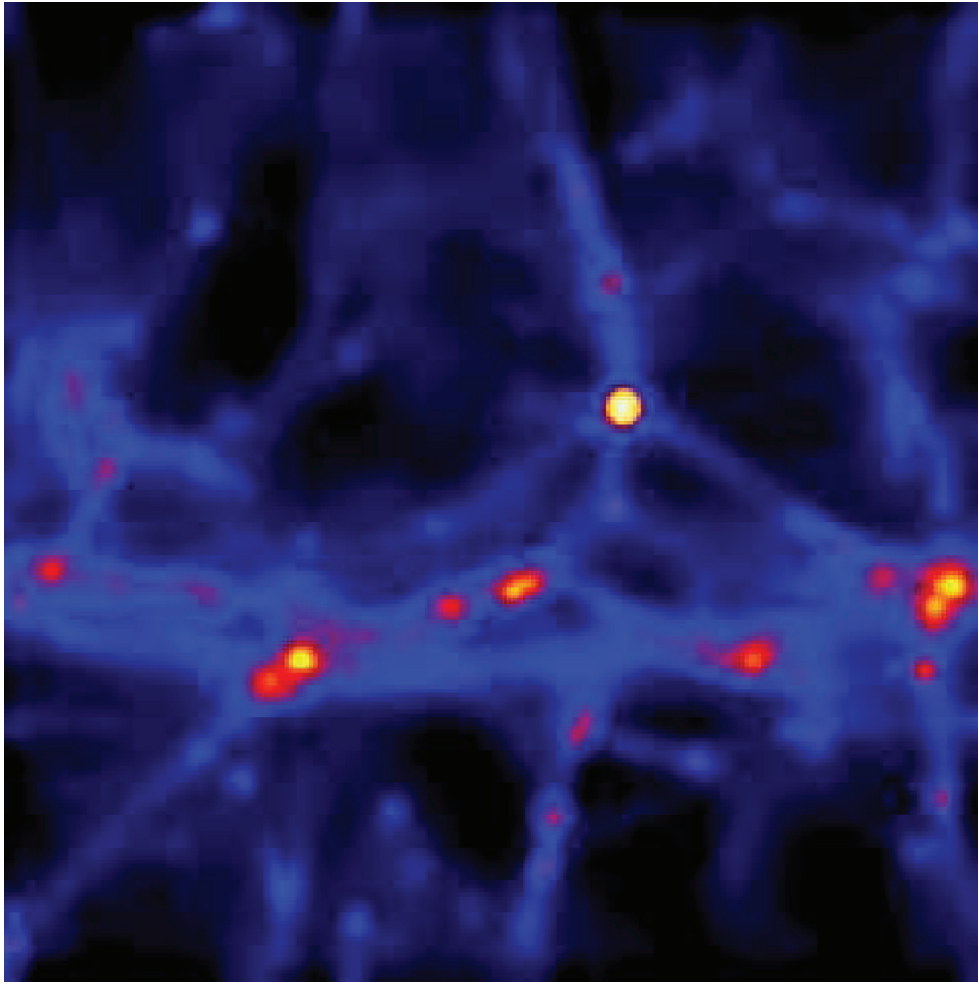


Fig. 14.2. Density field within a standard Λ CDM cosmology at $z = 20$. The box has a physical size of ~ 10 kpc. Shown is the projected gas density (with darker shades corresponding to lower density), which closely follows the dynamically dominant dark-matter component. The bright knots at the intersection of the filamentary network are the sites where the first stars formed, and where the first GRBs might have exploded (from Bromm *et al.* 2003).

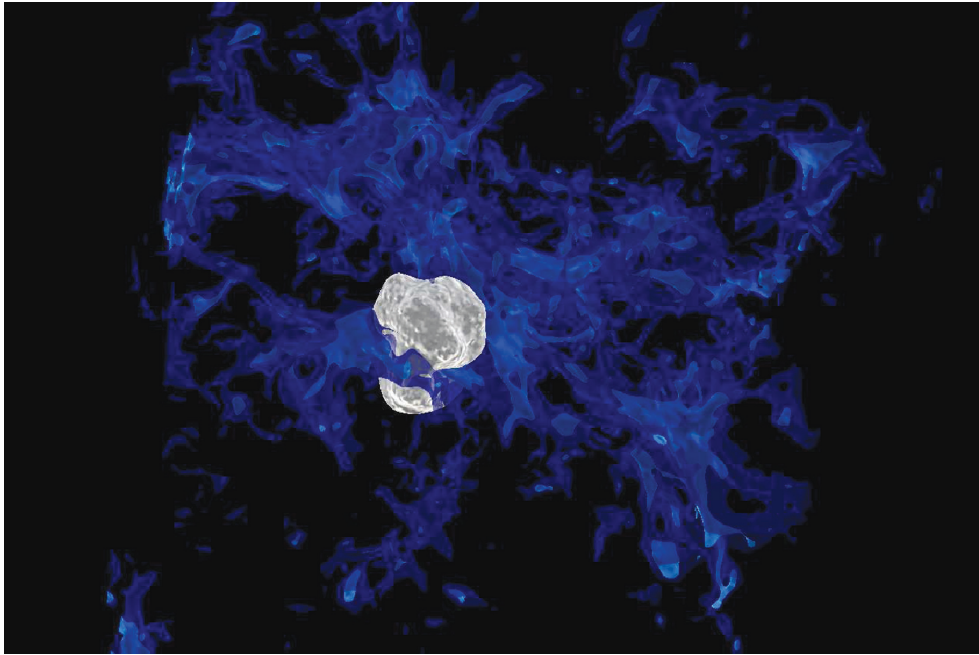


Fig. 14.4. Radiative feedback from the first stars (adopted from Johnson *et al.* 2007). The dark contours show the density field at $z \sim 20$ within a cosmological box of physical size ~ 30 kpc. At the center of the box, a single Pop III star with $100 M_{\odot}$ has formed, creating a bubble of ionized radiation (white contour) that reaches a maximum size of ~ 5 kpc (physical). The radiative feedback is fairly localized in extent, and leaves much of the surrounding IGM undisturbed. This snapshot shows the situation that would be present just before the Pop III star dies, possibly triggering a GRB explosion in the process. (Visualization courtesy of Paul Navrátil at the Texas Advanced Computing Center.)

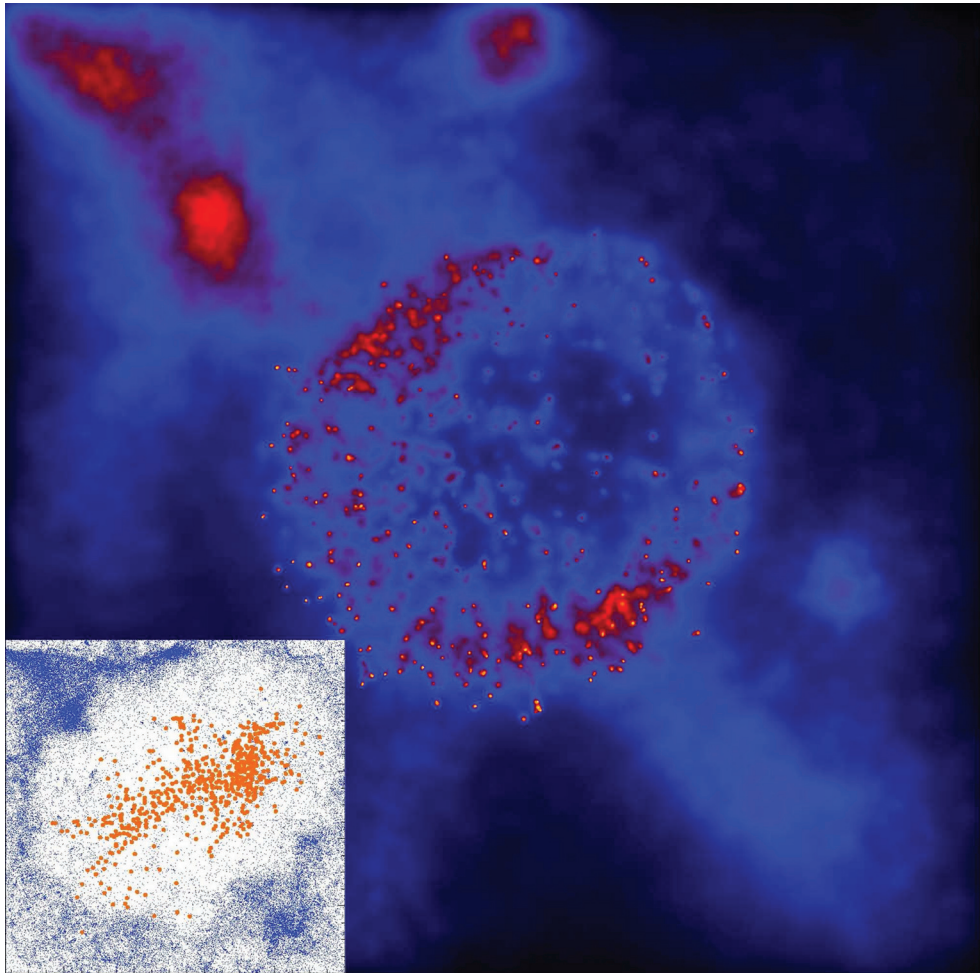


Fig. 14.5. Chemical feedback from the first stars (adopted from Bromm *et al.* 2003). SN explosion in the high-redshift Universe that ends the life of a $200 M_{\odot}$ Pop III star. The snapshot is taken $\sim 10^6$ yr after the explosion with total energy $E_{\text{SN}} \simeq 10^{53}$ erg. We show the projected gas density within a box of linear size 1 kpc. The SN bubble has expanded to a radius of ~ 200 pc, having evacuated most of the gas in the mini-halo. *Inset:* Distribution of metals. The stellar ejecta (red dots) trace the metals and are embedded in pristine metal-poor gas (blue dots). (Reproduced with permission from the AAS.)